Aluminophosphate Waste Forms for Immobilizing Cations from Electrochemical Salt Wastes

Nuclear Technology Research and Development

Prepared for U.S. Department of Energy Material Recovery and Waste Form Development Campaign

B.J. Riley, S. Chong, M. Peterson, and E.T. Nienhuis Pacific Northwest National Laboratory February 3, 2023 PNNL-33906



DISCLAIMER

This information was prepared as an account of work sponsored by an agency of the U.S. Government. Neither the U.S. Government nor any agency thereof, nor any of their employees, makes any warranty, expressed or implied, or assumes any legal liability or responsibility for the accuracy, completeness, or usefulness, of any information, apparatus, product, or process disclosed, or represents that its use would not infringe privately owned rights. References herein to any specific commercial product, process, or service by trade name, trademark, manufacturer, or otherwise, does not necessarily constitute or imply its endorsement, recommendation, or favoring by the U.S. Government or any agency thereof. The views and opinions of authors expressed herein do not necessarily state or reflect those of the U.S. Government or any agency thereof.

SUMMARY

This report provides experimental details and results of evaluating aluminophosphate waste forms for treating and immobilizing the salt cations from salt wastes generated during electrochemical reprocessing of used nuclear fuel. In the waste form process for these materials, chloride salt streams are reacted with NH₄H₂PO₄, the chlorine is removed from the salts and driven off as NH₄Cl (a solid condensate that can be captured), and then the product can be vitrified in conjunction with glass-forming chemicals (e.g., Fe₂O₃, Al₂O₃) to create a highdurability waste form. This study was initiated with some literature review on aluminophosphates containing high alkali oxide content and some of this information is summarized in this report. Following literature review, three new samples were synthesized where two contained Fe₂O₃+Al₂O₃ (i.e., samples **G3** and **G5**) and one was only Al₂O₃ (Fe₂O₃-free) (i.e., sample **G6**). In addition to these samples, G1 was also made, which is the baseline reference waste form referred to as DPF5-336 (made without Al₂O₃). Samples G1, G3, G5, and G6 had phases of Li₃Fe₂(PO₄)₃ (likely), monazite (below XRD detection limits), AlPO₄, and AlPO₄, respectively. Characterizations on these materials included optical images, scanning electron microscopy, energy dispersive X-ray spectroscopy, and X-ray diffraction. These samples were shipped to Argonne National Laboratory for chemical durability testing. Depending on how the samples perform in these tests, an additional phase of aluminophosphate formulations could be designed and tested. This report completes the milestone M4FT-23PN030104041 with details provided in Appendix B.

CONTENTS

SUM	MARY	iii
ACR	ONYMS AND ABBREVIATIONS	ix
1.0	Introduction	1
2.0	Literature Review and Glass Compositions	2
3.0	Experimental Methods	6
4.0	Results and Discussion 4.1 Results for Sample G1 4.2 Results for Sample G3 4.3 Results for Sample G5 4.4 Results for Sample G6	7 10 14
5.0	Summary and Conclusions	20
6.0	Acknowledgements	21
7.0	References	22
Appe	endix A: XRD Information	26
Appe	endix B: Milestone Details	28
	FIGURES	
Figu	re 1. Summary of dissolution rate (<i>DR</i> in g/m²/d) of aluminophosphate glasses in the literature containing alkali oxides where data is presented both as log ₁₀ (bottom <i>x</i> -axis) and without log (top <i>x</i> -axis) where the compositions listed are in mol% with the balance being P ₂ O ₅ (Brow 1993; Karabulut et al. 2001a; Metwalli and Brow 2001; Moreau et al. 2009; Chenu et al. 2012; El Damrawi et al. 2020). Data are sorted by <i>DR</i> and color-coded based on Al ₂ O ₃ content (see legend for more information). Test temperatures are listed in brackets [] next to the citation.	3
Figu	re 2. Summary of dissolution rate (<i>DR</i> in g/m²/d) of aluminophosphate glasses in the literature containing alkaline earth oxides where data is presented both as log ₁₀ (bottom <i>x</i> -axis) and without log (top <i>x</i> -axis) where the compositions listed are in mol% with the balance being P ₂ O ₅ (El Hadrami et al. 2002, 2003; Kapoor et al. 2019; Karabulut et al. 2001a; Metwalli and Brow 2001). Data are sorted by <i>DR</i> and color-coded based on Al ₂ O ₃ content (see legend for more information). Test temperatures are listed in brackets [] next to the citation.	Л
Figu	re 3. Optical collage of G1, G3, G5, and G6 glasses after quenching	

Figure 4. SEM micrographs for G1 at (a) 100×, (b) 150×, and (c) 2000× magnifications. The shadow in (a) is an artifact from the backscattered electron (BSE) detector	8
Figure 5. SEM-EDS dot map for G1 including the SEM micrograph, EDS overlay, and the elemental maps for P, Fe, K, O, and Na.	8
Figure 6. SEM micrograph with EDS spot analysis regions for G1 at the top of the sample where the phase separation meets the bulk matrix phase with data presented in Table 6	8
Figure 7. XRD data for the quenched DPF5-336 reference materials including (top pattern; sample G1) after vitrification using oxides, carbonates, and ADP and (bottom pattern) the same composition made by dechlorinating ERV3b salt followed by vitrification; see Riley et al. (2023) for more information. While both samples appear mostly amorphous, small peaks marked with red dots fit the ICDD pattern for Li ₃ Fe ₂ (PO ₄) ₃ (see inset plot shown with background subtracted).	10
Figure 8. SEM micrographs for G3 at (a) 150×, (b) 300×, and (c) 2000× magnifications	11
Figure 9. SEM-EDS dot map for G3 including the SEM micrograph and the elemental maps for P, Fe, K, O, Al, K, Na, and Cs	11
Figure 10. SEM micrograph with EDS spot analysis regions for G3 at the bottom of the sample where the phase separation meets the bulk matrix phase with data presented in Table 7	11
Figure 11. SEM micrograph with EDS spot analysis regions for G3 at the top of the sample near the phase-separated region (low magnification) with the data presented in Table 8	12
Figure 12. SEM micrograph with EDS spot analysis regions for G3 at the top of the sample near the phase-separated region (high magnification), including some dendritic crystal growth, with data included in Table 9.	13
Figure 13. XRD data for the quenched G3 sample after vitrification. While monazite-type crystals were observed during SEM-EDS analysis, these are below detection limits of the XRD instrument.	14
Figure 14. SEM micrographs for G5 at (a) 100× (middle), (b) 100× (top), and (c) 2000× (top) magnifications.	14
Figure 15. SEM-EDS dot map for G5 including the SEM micrograph, EDS overlay, and the elemental maps for P, Fe, Al, Na, K, Cs, O, Sr, Ce, and Nd.	15
Figure 16. SEM micrograph with EDS spot analysis regions for G5 at the top of the sample where the phase separation meets the bulk matrix phase with data presented in Table 10	15
Figure 17. XRD data for the quenched G5 sample after vitrification (peaks at 19.5° 20, 22.5° 20, and 34° 20 remain unidentified).	16
Figure 18. SEM micrographs for G6 at (a) 100×, (b) 300×, and (c) 1000× magnifications	17
Figure 19. SEM-EDS dot map for G6 including the SEM micrograph, EDS overlay, and the elemental maps for P, Fe, Al, Na, K, Cs, O, Sr, Ce, and Nd	17
Figure 20. SEM micrograph with EDS spot analysis regions for G6 in the middle of the sample where the light matrix phase is distinctly different from the dark (AlPO ₄) inclusion phases – EDS data is presented in Table 11.	18
Figure 21. XRD data for the quenched G6 sample after vitrification.	19
Figure 22. Picture of G6 on white background so the blueish-purple color is easier to observe	19

TABLES

Table 1. Summary of the ERV3b salt composition (mass%)	1
Table 2. Expected composition of DPF5-336 glass after oxide conversion (mass%). The salt-cation-oxide (SCO) loading in this waste form is 19.62 mass%.	1
Table 3. Summary of various studies in the literature on aluminophosphate glasses with cited literature values	2
Table 4. Compositions (mass%) of glasses in this study (ID = identification). The additive $NH_4H_2PO_4$ is also referred to as ADP (ammonium dihydrogen phosphate), SCO denotes salt cation oxide loading, and T_m is the melting temperature used to vitrify the sample (hold time was 1 hour at the temperature)	5
Table 5. Details of the reagents used in the current study to fabricate samples	6
Table 6. Summary of EDS spot analysis results (atomic%) from G1 (see Figure 6) including the homogeneous matrix phase (regions 1-5) and phase-separated phase (regions 6-10) as well as average (ave) and standard deviation (SD) data for like regions	9
Table 7. Summary of EDS spot analysis results (atomic%) from the bottom G3 (see Figure 10) including average (ave) and standard deviation (SD) data for like regions	12
Table 8. Summary of EDS spot analysis results (atomic%) from the top (high magnification) region of G3 (see Figure 11)	12
Table 9. Summary of EDS spot analysis results (atomic%) from G3 (see Figure 12) with separate datasets for the matrix phase (light gray – regions 1-3), dark gray phase (regions 4-6), and the bright phase at the top (regions 7-9) including average (ave) and standard deviations (SD) for the like regions.	13
Table 10. Summary of EDS spot analysis results (atomic%) from G5 (see Figure 16) including the homogeneous matrix phase (regions 1-3) and the heterogeneous and phase-separated region (regions 4-6) including average (ave) and standard deviation (SD) data for like regions.	16
Table 11. Summary of spot EDS data (atomic%) for G6 with regions called out in Figure 20 including average (ave) and standard deviation (SD) data for like regions	18
APPENDIX TABLES:	
Table A1. Summary of phases identified during XRD analysis including the powder diffraction file (PDF) numbers from the ICDD database, the space group (SG; and SG number), and the unit cell parameters in Angstroms (Å)	27

viii

ACRONYMS AND ABBREVIATIONS

ADP ammonium dihydrogen phosphate (i.e., NH₄H₂PO₄)

ANL Argonne National Laboratory

ASTM American Society for Testing and Materials (International)

BSE backscattered electron (detector for SEM)

DOE Department of Energy

DPF dehalogenated phosphate waste form with Fe₂O₃

EBR-II Experimental Breeder Reactor-II
EDS energy dispersive X-ray spectroscopy
ERV3b electrorefiner salt simulant version 3b

FY fiscal year G# glass number

ICDD International Centre for Diffraction Data

ID identification

INL Idaho National Laboratory

m mass basis M molar basis

MRWFD Material Recovery and Waste Form Development (Campaign)

NEUP Nuclear Energy University Partnership (Program)

NS no salt (samples made from oxides, carbonates, and ADP)

PCT product consistency test PDF powder diffraction file

PNNL Pacific Northwest National Laboratory

SCO salt cation oxide

SD standard deviation ($\pm 1\sigma$) SEM scanning electron microscopy

SG space group

 $T_{\rm m}$ melting temperature

U.S. United StatesXRD X-ray diffraction

1.0 Introduction

Efforts under the Material Recovery and Waste Form Development (MRWFD) Campaign under the Department of Energy (DOE) Office of Nuclear Energy are aimed at formulating, fabricating, and evaluating performance for waste form concepts designed to immobilize salt wastes from electrochemical reprocessing of used Experimental Breeder Reactor-II (EBR-II) fuel (Vienna et al. 2015; Ebert et al. 2017; Frank et al. 2017). This salt waste is mostly comprised of the LiCl-KCl eutectic salt but also contains NaCl (from bond Na in the fuel) and chlorides of the fission products from the fuel.

Options for immobilizing this salt waste stream include (1) full salt incorporation into a single waste form (e.g., glass-bonded sodalite) (Ebert 2005; Bateman et al 2007; Riley et al. 2017) or (2) partitioning the salt and putting different waste streams into different forms for disposal (Siemer 2012; Riley et al. 2020, 2021). For option (2), dehalogenation (halogen removal through chemical reactions) can be used to remove the halogen content from the salt, which allows for different waste form options than are possible without dehalogenation due to low halide solubility limits in traditional nuclear waste forms (e.g., borosilicate glass) and retention during high-temperature melting (Hrma 2010; Riley et al. 2012, 2014).

While a lot of recent work has been conducted looking at dehalogenating processes for these salts using phosphate compounds and immobilizing the dechlorinated product in an iron phosphate waste form (Ebert and Fortner 2019a, 2019b; Riley and Chong 2020, 2022a, 2022b; Riley et al. 2019, 2020, 2023; Stariha and Ebert 2020, 2021), an alternative option to using Fe₂O₃ as the glass stabilization additive is to use a mixture of Fe₂O₃+Al₂O₃ or Al₂O₃ alone (without Fe₂O₃). The aim of this report is to provide documentation for experiments that were performed to evaluate aluminophosphate formulations for the electrorefiner salt (version 3b) waste simulant ERV3b (see Table 1). Included in this report are documentation of the formulations used, the processes used to make the selected compositions, and characterization of those samples. While both iron phosphates and aluminophosphates have been studied for many years, no literature was found with compositions closely resembling those expected from dechlorinating ERV3b with ammonium dihydrogen phosphate (ADP) such as the DPF5-336 reference material with a salt-cation-oxide loading of 19.62 mass% (Ebert and Fortner 2019a, 2019b; Riley and Chong 2020, 2022a, 2022b; Riley et al. 2019, 2020; Stariha and Ebert 2020, 2021) with the target composition shown in Table 2.

Table 1. Summary of the ERV3b salt composition (mass%).

Constituent	LiCl	KCl	NaCl	CsCl	$SrCl_2$	CeCl ₃	$NdCl_3$
ERV3b	32.05	39.06	9.01	7.01	3.00	5.00	4.87

Table 2. Expected composition of DPF5-336 glass after oxide conversion (mass%). The salt-cation-oxide (SCO) loading in this waste form is 19.62 mass%.

Oxide	P_2O_5	Fe ₂ O ₃	Li ₂ O	K ₂ O	Na ₂ O	Cs ₂ O	SrO	CeO ₂	Nd ₂ O ₃
Mass%	46.28	34.10	4.00	8.75	1.69	2.08	0.70	1.24	1.16

This work has been done through a collaborative effort between Pacific Northwest National Laboratory (PNNL), Argonne National Laboratory (ANL), and Idaho National Laboratory (INL) including a range of staff across these complexes with support and advisory support from various contributors outside the United States National Laboratory DOE complex including U.S. universities (see Acknowledgements in Section 6.0).

2.0 Literature Review and Glass Compositions

To start this process, a literature review was initiated to assess the state of the art in the area of alumina-containing phosphate and alumina-containing iron phosphate waste forms with the focus on the former and a list of several studies is included in Table 3. Additionally, while chemical durability data was the primary focus aside from finding similar compositions, very little data was found in the literature for chemical durability tests run under standardized test conditions such as those approved by the American Society for Testing and Materials (ASTM) International procedures like the C1285 (product consistency test or PCT) or C1308 (coupon test in dilute conditions).

Table 3. Summary of various studies in the literature on aluminophosphate glasses with cited literature values.

Glass compositions (mol%)	Reference(s)
x Al(PO ₃) ₃ •(1- x)NaPO ₃ [$0 \le x \le 0.25$]	Brow (1993)
$xAlPO_4 \cdot (1-x)NaPO_3; 0 \le x \le 0.125$	Brow (1993)
$xAl_2O_3 \cdot (1-x)NaPO_3; 0 \le x \le 0.275$	Brow (1993)
x NaAlO ₂ •(1- x)NaPO ₃ ; $0 \le x \le 0.20$	Brow (1993)
$40\text{Na}_2\text{O} \cdot (20-x)\text{Al}_2\text{O}_3 \cdot x\text{Fe}_2\text{O}_3 \cdot 40\text{P}_2\text{O}_5; 5 \le x \le 20$	Glazkova et al. (2017)
$Na_2O \bullet Al_2O_3 \bullet P_2O_5 \bullet B_2O_3$	Donald et al. (2006)
x NaPO ₃ •0.5(95- x)ZnO•0.5(95- x)Nb ₂ O ₅ •5Al ₂ O ₃ ; 27.5 $\leq x \leq$ 47.5	Chenu et al. (2012)
$20\text{Na}_2\text{O} \cdot 5\text{Al}_2\text{O}_3 \cdot x\text{TiO}_2 \cdot (45-x)\text{Nb}_2\text{O}_5 \cdot 30\text{P}_2\text{O}_5; 15 \le x \le 45$	Teixeira et al. (2007)
$(100-x)(50P_2O_5 \cdot 15ZnO \cdot 15PbO \cdot 20CdO) - xAl_2O_3; x = 6.8$	El Hadrami et al. (2002, 2003)
$xAl_2O_3 \bullet (40-x)Ag_2O \bullet 60P_2O_5; 0 \le x \le 20$	El Damrawi et al. (2020)
$50\text{Li}_2\text{O}\bullet x\text{Al}_2\text{O}_3\bullet (50-x)\text{P}_2\text{O}_5; 2 \le x \le 5$	Moreau et al. (2009)
30CaO•10Al ₂ O ₃ •60P ₂ O ₅	Kapoor et al. (2019)
$(35-x)$ CaO• x Al ₂ O ₃ •P ₂ O ₅ ; $0 \le x \le 15$	Liu et al. (2016)
35 CaO• x Al ₂ O ₃ • $(65-x)$ P ₂ O ₅ ; $0 \le x \le 12.5$	Liu et al. (2016)
$(25-x)\text{La}_2\text{O}_3 \bullet x\text{Al}_2\text{O}_3 \bullet 75\text{P}_2\text{O}_5$	Karabulut et al. (2001b)
(30-x)La ₂ O ₃ • x Al ₂ O ₃ • 70 P ₂ O ₅	Karabulut et al. (2001b)
$20\text{Na}_2\text{O} \cdot (20-x)\text{Al}_2\text{O}_3 \cdot x\text{Fe}_2\text{O}_3 \cdot 60\text{P}_2\text{O}_5; \ 0 \le x \le 20$	Karabulut et al. (2001a)
15ZnO• $(17.5-x)$ Al ₂ O ₃ • x Fe ₂ O ₃ • 67.5 P ₂ O ₅ ; $x = 7.5$, 12.5	Karabulut et al. (2001a)
50P2O5 • (50-x)ZnO • xAl2O3	Li et al. (2015)
$50P_2O_5-20Al_2O_3-(30-x)ZnO-xZrO_2$	Li et al. (2015)
$xAl(PO_3)_3 \bullet (1-x)KPO_3$	Metwalli and Brow (2001)
$xAl(PO_3)_3 \bullet (1-x)Mg(PO_3)_2$	Metwalli and Brow (2001)
xAl(PO ₃) ₃ •(1- x)Ba(PO ₃) ₂	Metwalli and Brow (2001)
$Na_2O \bullet K_2O \bullet Li_2O \bullet BaO \bullet CaO \bullet ZnO \bullet SnO \bullet B_2O_3 \bullet Sb_2O_3 \bullet Al_2O_3 \bullet P_2O_5$	Marino et al. (2001)

Regarding chemical durability tests, some data was found in the literature on aluminophosphates, but the tests run on these glasses varied extensively. Thus, the data presented below in Figure 1 and Figure 2 include data solely based on dissolution rates (or mass lost) for alkali-containing and alkaline-earth-containing aluminophosphate glasses, respectively. For the data plotted in Figure 1, it is clear that the dissolution rates vary extensively (nearly 14 orders of magnitude) across the data available, but again, these glasses are difficult to compare on a 1-to-1 basis considering that test conditions (e.g., reaction time, reaction

temperature, sample morphology) were not consistent or standardized, compositions were not consistent across this dataset, and the studies were done independently by different research organizations.

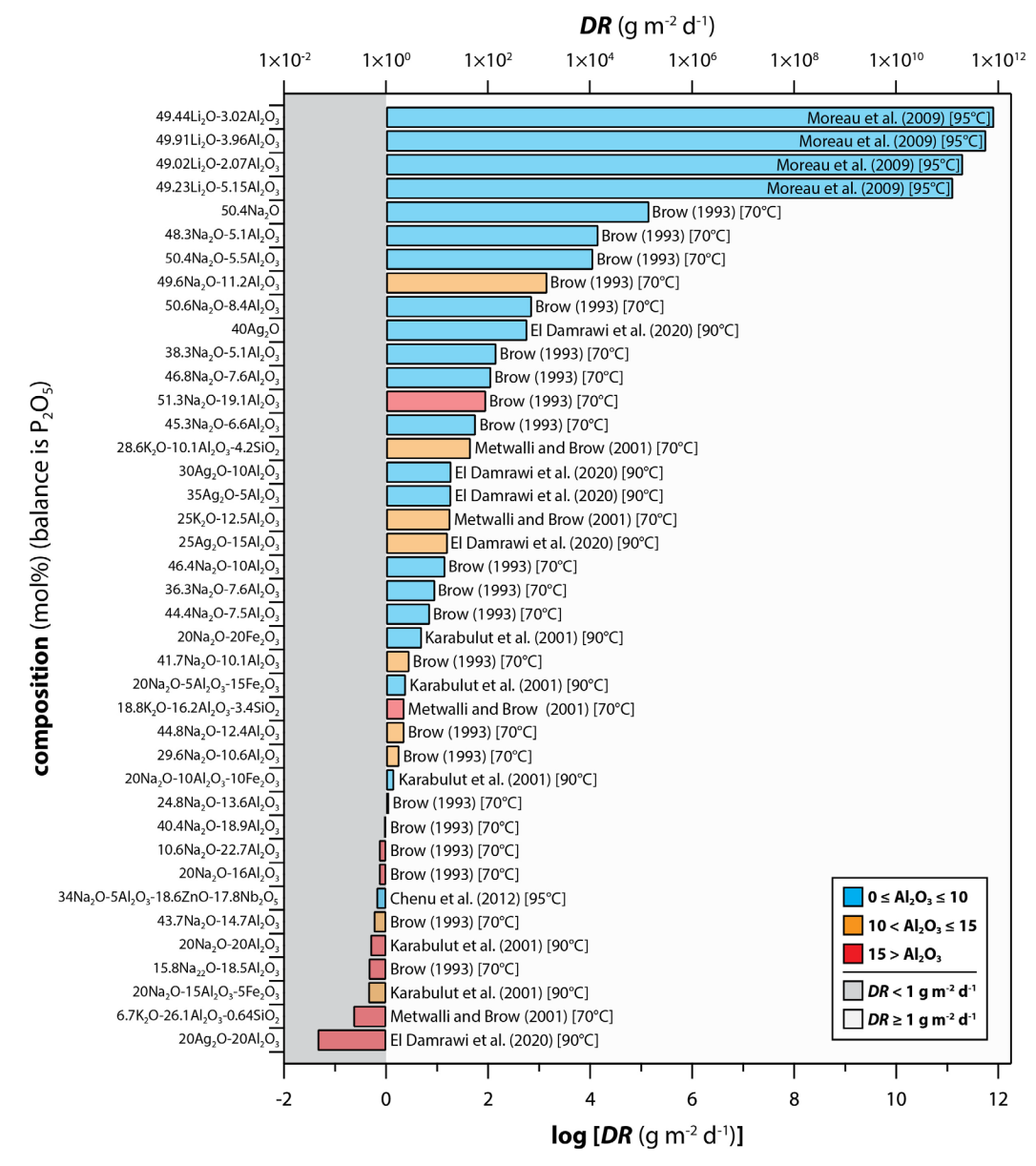


Figure 1. Summary of dissolution rate (*DR* in g/m²/d) of aluminophosphate glasses in the literature containing alkali oxides where data is presented both as log₁₀ (bottom x-axis) and without log (top x-axis) where the compositions listed are in mol% with the balance being P₂O₅ (Brow 1993; Karabulut et al. 2001a; Metwalli and Brow 2001; Moreau et al. 2009; Chenu et al. 2012; El Damrawi et al. 2020). Data are sorted by *DR* and color-coded based on Al₂O₃ content (see legend for more information). Test temperatures are listed in brackets [] next to the citation.

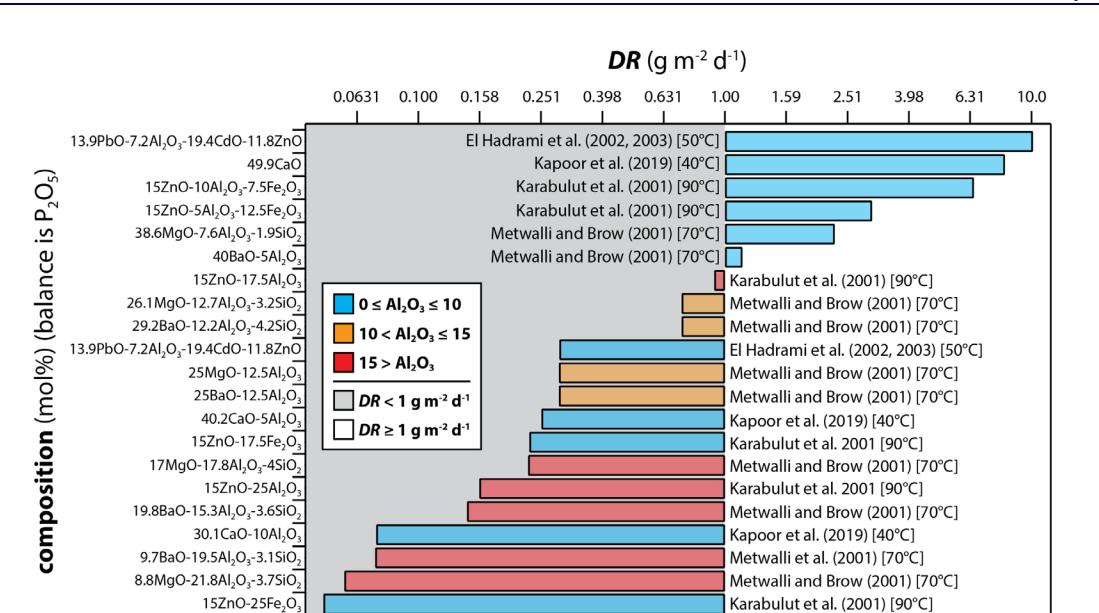


Figure 2. Summary of dissolution rate (*DR* in g/m²/d) of aluminophosphate glasses in the literature containing alkaline earth oxides where data is presented both as log₁₀ (bottom x-axis) and without log (top x-axis) where the compositions listed are in mol% with the balance being P₂O₅ (El Hadrami et al. 2002, 2003; Kapoor et al. 2019; Karabulut et al. 2001a; Metwalli and Brow 2001). Data are sorted by *DR* and color-coded based on Al₂O₃ content (see legend for more information). Test temperatures are listed in brackets [] next to the citation.

-0.6

-0.4

-0.2

 $\log [DR (q m^{-2} d^{-1})]$

-1.2

-1.0

-0.8

0.0

0.2

0.4

0.6

0.8

1.0

The compositions for the four glasses in the current study are shown in Table 4. Based on the limited chemical durability data in the literature fitting the specific needs of this activity, the initial approach for this work was to start with the DPF5-336 reference composition (sample G1) (Riley and Chong 2022a; Stariha and Ebert 2022) and perform systematic compositional variations from that starting point on a mass (sample G3) and molar (sample G5) basis.

For this study, all samples were made starting from ammonium dihydrogen phosphate (ADP or NH₄H₂PO₄), oxides, and carbonates instead of starting from ADP, Fe₂O₃, and salt simulants. The G3 glass is the same composition as G1 but with a 50/50 split of Fe₂O₃/Al₂O₃ (mass basis). The G5 glass is a 50/50 split of Fe₂O₃/Al₂O₃ (molar basis) with all other components being adjusted accordingly where the salt cation oxide (SCO) loading was the highest of the four samples. The G6 sample is the only one in the study without Fe₂O₃ where all components remained fixed (mass basis) except P₂O₅ and Al₂O₃ where the P₂O₅:(Fe₂O₃+Al₂O₃) mass ratio is 4.23 instead of 1.36 for the G1 and G3 samples. For G6, one other Fe₂O₃-free glass was attempted with a higher Al₂O₃:P₂O₅ molar ratio, but it turned out very heterogeneous so the G6 formulation was selected for further study.

Table 4. Compositions (mass%) of glasses in this study (ID = identification). The additive $NH_4H_2PO_4$ is also referred to as ADP (ammonium dihydrogen phosphate), SCO denotes salt cation oxide loading, and T_m is the melting temperature used to vitrify the sample (hold time was 1 hour at the temperature).

Component	Reagent	G1	G3	G5	G6
P_2O_5	NH ₄ H ₂ PO ₄	46.283	46.283	49.323	65.000
Fe ₂ O ₃	Fe ₂ O ₃	34.102	17.051	18.171	0.000
Al ₂ O ₃	Al ₂ O ₃	0.000	17.051	11.602	15.385
Li ₂ O	Li ₂ CO ₃	4.003	4.003	4.266	4.003
K ₂ O	K ₂ CO ₃	8.746	8.746	9.321	8.746
Na ₂ O	Na ₂ CO ₃	1.694	1.694	1.805	1.694
Cs ₂ O	Cs ₂ CO ₃	2.08	2.08	2.216	2.08
SrO	SrCO ₃	0.694	0.694	0.74	0.694
CeO ₂	CeO ₂	1.239	1.239	1.321	1.239
Nd_2O_3	Nd ₂ O ₃	1.158	1.158	1.234	1.158
SUM	_	100.00	100.00	100.00	100.00
SCO		19.62	19.62	20.90	19.62
Sample IDs	_	(a)	(b)	(c)	(d)
P:(Fe+Al) ^(e)	_	1.36	1.36	1.66	4.23
T _m (°C)	_	1100	1300	1300	1200

⁽a)DPF5-336ref-NS (G1); (b)50Fe-50Al-m (G3); (c)50Fe-50Al-M (G5); (d)alt-100Al (G6); (e)ratios in mass% for oxides. Note that, within the sample filenames, "NS" denotes no salt, "m" denotes mass-basis, and "M" denotes molar basis.

3.0 Experimental Methods

3.1 Batching and Melting

Glasses were batched starting from ADP, Fe₂O₃, Al₂O₃, Li₂CO₃, K₂CO₃, Na₂CO₃, Cs₂CO₃, SrCO₃, CeO₂, and Nd₂O₃. Reagents were batched using plastic weigh boats and Mettler Toledo balances, they were loaded into a 250 mL alumina conical crucible (ACC3742, McDanel Advanced Ceramic Technologies), and mixed together. Samples were melted in a high-temperature Deltech furnace using 5°C/min ramp rates, dwelled for 1-hour at the melting temperature (*T*_m) (see Table 4), and then were poured onto an Inconel quench plate.

Component	Reagent	Vendor	Lot#	Purity (%)
P_2O_5	NH ₄ H ₂ PO ₄	Sigma Aldrich	SLBZ2580	≥98.5
Fe ₂ O ₃	Fe ₂ O ₃	Baker	00007507	103
Al ₂ O ₃	Al ₂ O ₃	Alfa Aesar	R06G041	99
Li ₂ O	Li ₂ CO ₃	Alfa Aesar	N27G037	99
K ₂ O	K ₂ CO ₃	Alfa Aesar	U17E036	99
Na ₂ O	Na ₂ CO ₃	Sigma Aldrich	051M0107V	99.95
Cs ₂ O	Cs ₂ CO ₃	Sigma Aldrich	0000025335	99.995
SrO	SrCO ₃	Sigma Aldrich	MKBZ1178V	99.9
CeO ₂	CeO ₂	Alfa Aesar	Z17E046	99.9
Nd_2O_3	Nd_2O_3	Alfa Aesar	S06A013	99.9

Table 5. Details of the reagents used in the current study to fabricate samples.

3.2 Sample Characterization

Upon quenching, pictures were taken of the materials with a digital camera. For the sample characterizations, a piece of each quenched material was mounted in resin and polished so a cross-section could be observed with scanning electron microscopy (SEM) and energy dispersive X-ray spectroscopy (EDS) using a JSM-7001F field emission gun SEM (JEOL USA) and an xFlash 6|60 EDS detector (Bruker AXS Inc.). The EDS characterizations included dot mapping and spot analyses. Portions of each sample were ground to a fine particle size in a tungsten carbide milling chamber and diffraction patterns were collected with a Bruker D8 Advance X-ray diffractometer (XRD) or Rigaku SmartLab Studio II – both instruments contained Cu X-ray sources.

⁽a) Mettler Toledo balances included an XPE with 220 g maximum mass and a PR with 2100 g maximum mass.

4.0 Results and Discussion

Pictures of the four different glasses are provided in Figure 3. Glasses G1, G3, and G5 all appeared black and opaque where G1 and G5 had reflective layers on the top surfaces and G3 appeared mostly homogeneous. The G6 glass was light whitish in color and appeared heterogeneous.



Figure 3. Optical collage of G1, G3, G5, and G6 glasses after quenching.

4.1 Results for Sample G1

The G1 sample had some phase-separated regions on the top of the sample as shown in Figure 4, Figure 5, and Figure 6 with EDS data presented in Table 6. While the data in Table 6 suggest that the homogeneous matrix phase and the heterogeneous phase-separated regions are very similar in composition, it is possible that the differences in appearance between these are due to elements that are not detectable by EDS such as Li, which is present in high concentrations in these materials. Subtle differences are seen between these different regions that include Al content as well as K and Fe. It is also possible that these phases are not crystalline, although they appear to have faceted structures – the other possibility is that they are below the detection limits of the XRD instrument. The EDS dot map shown in Figure 5 provides evidence that the only elements fluctuating between the matrix and phase-separated regions are K, O and maybe Na (slightly) where the brighter matrix phase is higher in K and Na. The darker phase-separated region is likely lower in average atomic number based on the functionality of the backscattered electron detector used to collect this SEM micrograph and this fact also supports the presence of Li in this phase.

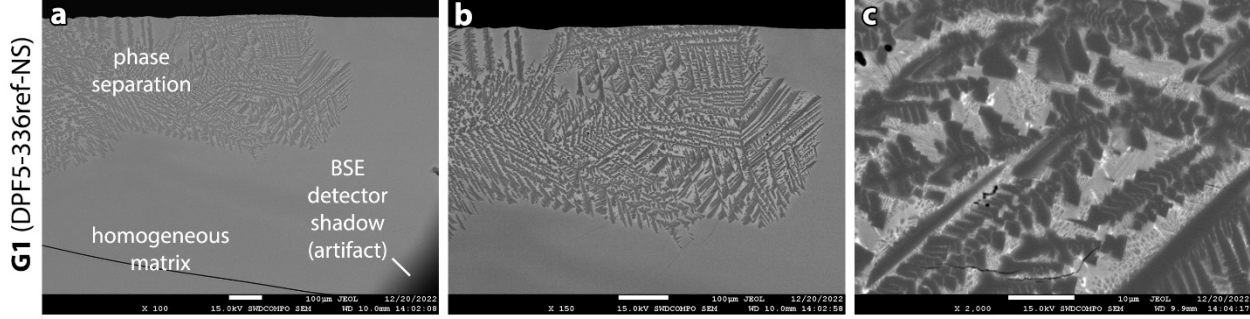


Figure 4. SEM micrographs for G1 at (a) 100×, (b) 150×, and (c) 2000× magnifications. The shadow in (a) is an artifact from the backscattered electron (BSE) detector.

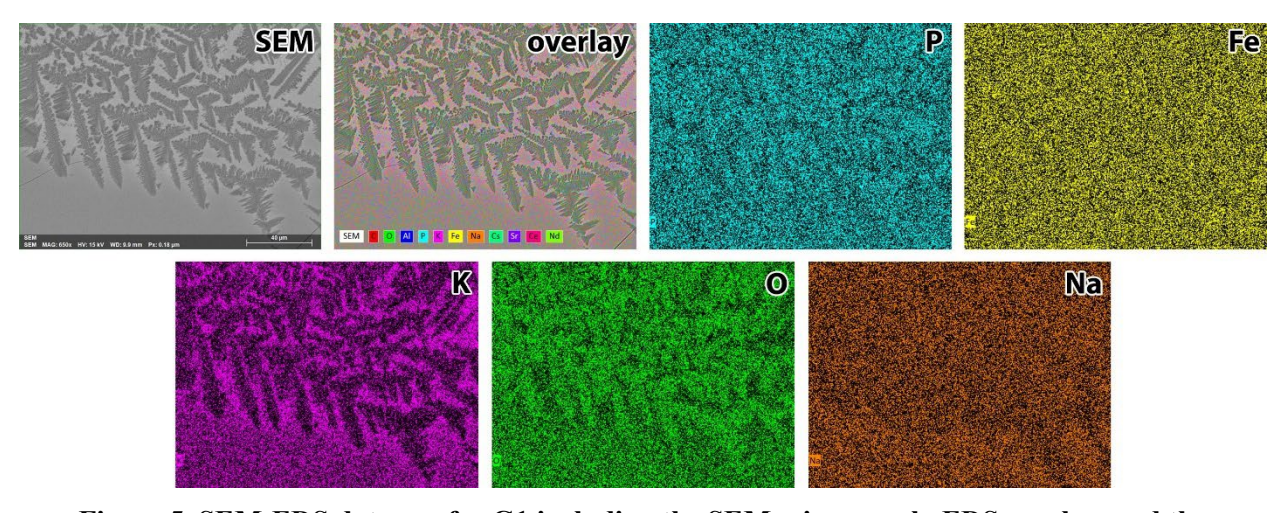


Figure 5. SEM-EDS dot map for G1 including the SEM micrograph, EDS overlay, and the elemental maps for P, Fe, K, O, and Na.

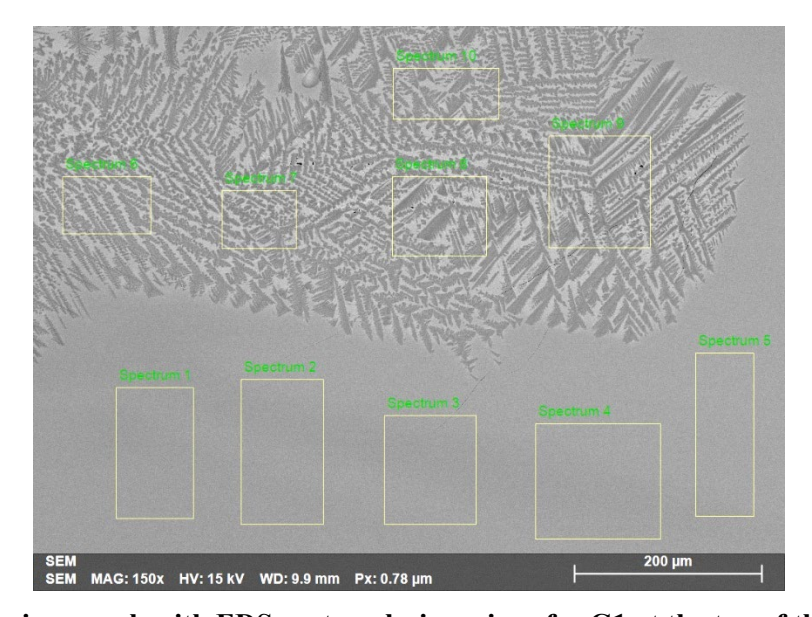


Figure 6. SEM micrograph with EDS spot analysis regions for G1 at the top of the sample where the phase separation meets the bulk matrix phase with data presented in Table 6.

Table 6. Summary of EDS spot analysis results (atomic%) from G1 (see Figure 6) including the homogeneous matrix phase (regions 1-5) and phase-separated phase (regions 6-10) as well as average (ave) and standard deviation (SD; $\pm 1\sigma$) data for like regions.

Region	О	Na	Al	P	K	Fe	Sr	Cs	Ce	Nd
reg-1	63.2	1.3	3.5	15.5	4.6	10.1	1.0	0.3	0.3	0.2
reg-2	63.1	1.3	3.4	15.6	4.5	10.1	1.1	0.3	0.4	0.2
reg-3	63.3	1.3	3.4	15.6	4.5	10.1	1.0	0.3	0.4	0.2
reg-4	63.6	1.2	3.2	15.8	4.5	9.9	1.1	0.3	0.3	0.2
reg-5	63.7	1.4	2.4	16.3	4.6	9.8	1.1	0.3	0.3	0.2
ave	63.4	1.3	3.2	15.8	4.5	10.0	1.0	0.3	0.3	0.2
SD	0.3	0.1	0.4	0.3	0.1	0.1	0.1	0.0	0.1	0.0
reg-6	63.9	1.2	2.0	16.0	4.8	10.2	1.1	0.3	0.3	0.2
reg-7	64.5	0.0	0.3	13.6	6.3	14.1	0.0	0.5	0.4	0.3
reg-8	63.6	1.4	2.0	16.2	4.6	10.4	1.0	0.2	0.4	0.2
reg-9	63.8	1.3	1.9	16.2	4.5	10.4	1.1	0.4	0.3	0.2
reg-10	64.1	1.4	2.3	15.6	4.8	9.8	1.1	0.4	0.3	0.2
ave	64.0	1.1	1.7	15.5	5.0	11.0	0.9	0.4	0.3	0.2
SD	0.4	0.6	0.8	1.1	0.7	1.8	0.5	0.1	0.1	0.0

The XRD data for G1 is provided in Figure 7 (starting from oxides, carbonates, and ADP) and is compared with the same composition made from Fe_2O_3 , ADP, and ERV3b salt simulant from a different study (Riley et al. 2023). The patterns both show broad amorphous diffraction peaks (humps) with some very small diffraction peaks that are attributed to a small quantity of crystalline material that fits well to the International Centre for Diffraction Data (ICDD) database pattern of $Li_3Fe_2(PO_4)_3$.

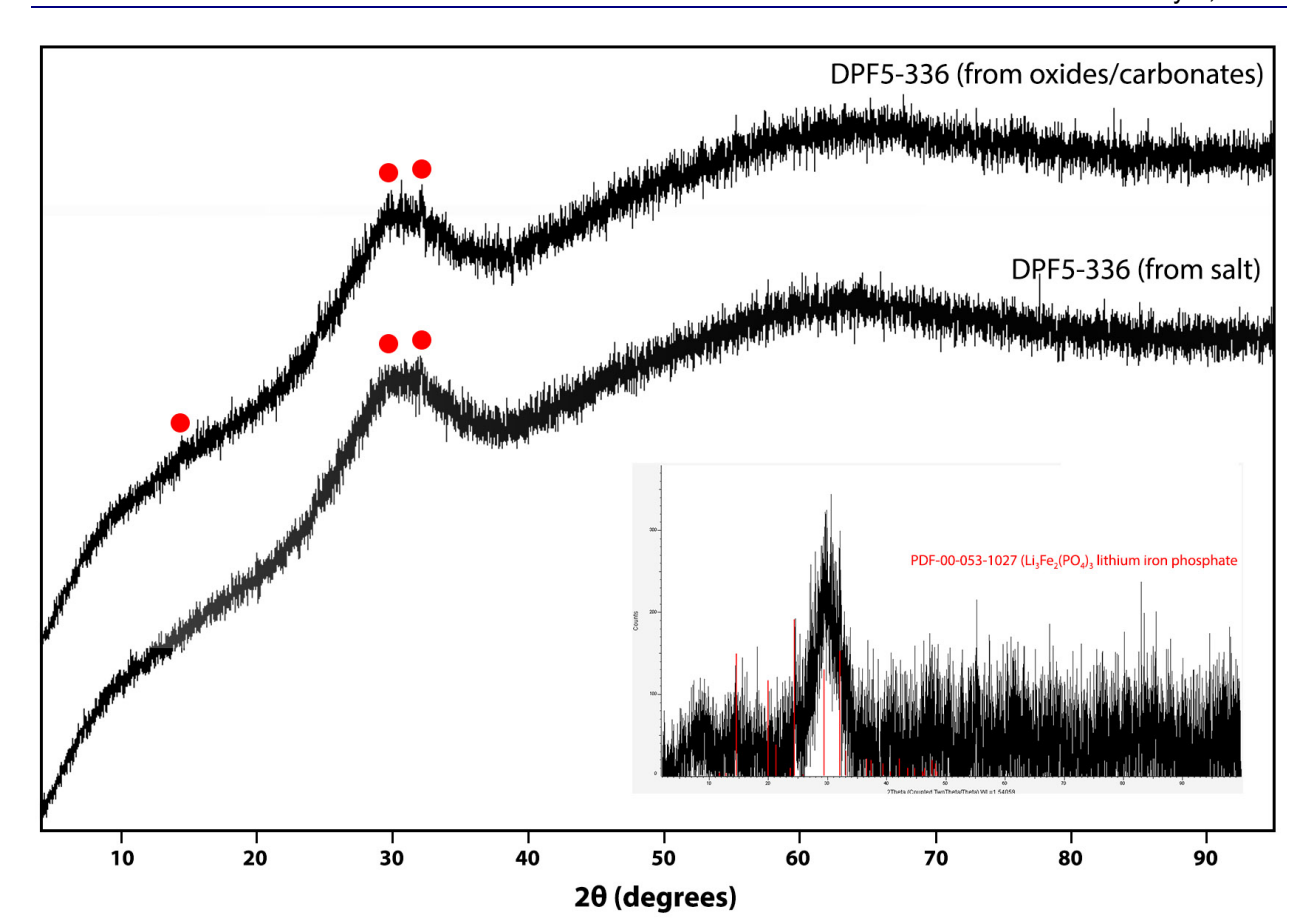


Figure 7. XRD data for the quenched DPF5-336 reference materials including (top pattern; sample G1) after vitrification using oxides, carbonates, and ADP and (bottom pattern) the same composition made by dechlorinating ERV3b salt followed by vitrification; see Riley et al. (2023) for more information. While both samples appear mostly amorphous, small peaks marked with red dots fit the ICDD pattern for Li₃Fe₂(PO₄)₃ (see inset plot shown with background subtracted).

4.2 Results for Sample G3

The results from SEM-EDS analysis on the G3 sample are provided in Figure 8, Figure 9, Figure 10, Figure 11, and Figure 12 as well as Table 7, Table 8, and Table 9. The majority of the G3 sample appeared very homogeneous, as seen in Figure 8a and Figure 10, but phase separation (and likely crystallization) was observed towards the top of the quenched material as can be seen in Figure 8b,c, Figure 9, Figure 11, and Figure 12 with some dendritic crystal growth. Based on the elemental EDS dot maps (Figure 9), the darker phase appears to be rich in Fe and Al whereas the alkali elements (K, Na, and Cs) are present in higher concentrations within the bulk matrix phase; this is corroborated by the data in Figure 12 and Table 9. The bright phase appears to be rich in Nd and Ce and is likely a monazite phase [i.e., (Nd,Ce)PO₄] based on the high P+O content.

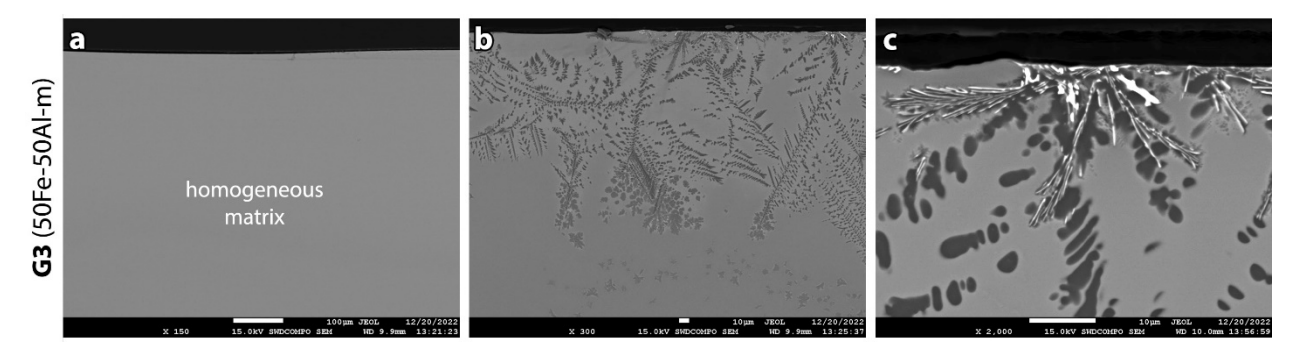


Figure 8. SEM micrographs for G3 at (a) 150×, (b) 300×, and (c) 2000× magnifications.

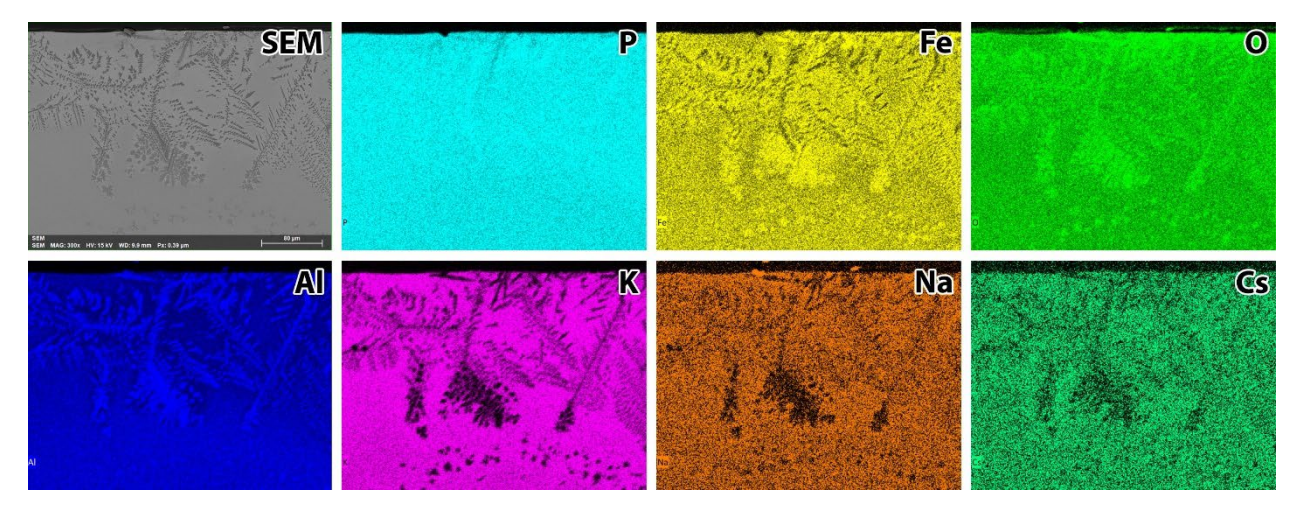


Figure 9. SEM-EDS dot map for G3 including the SEM micrograph and the elemental maps for P, Fe, K, O, Al, K, Na, and Cs.

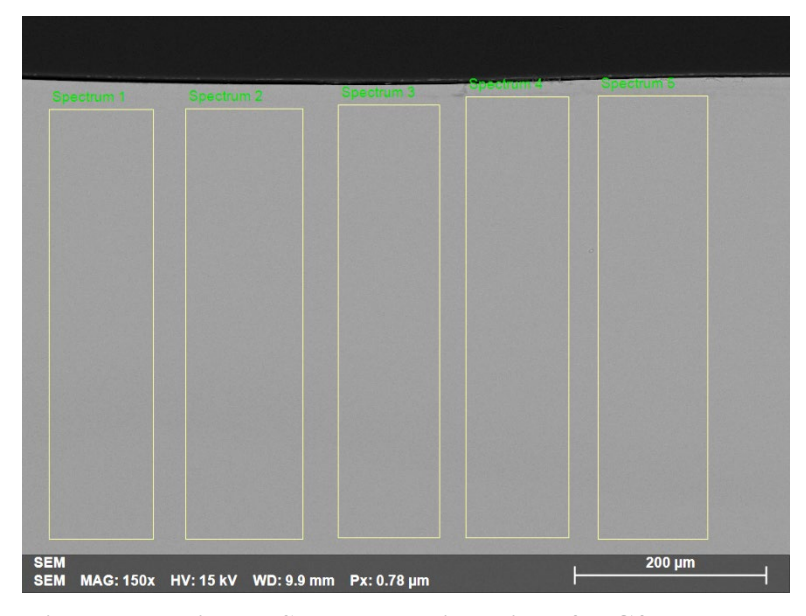


Figure 10. SEM micrograph with EDS spot analysis regions for G3 at the bottom of the sample where the phase separation meets the bulk matrix phase with data presented in Table 7.

Table 7. Summary of EDS spot analysis results (atomic%) from the bottom G3 (see Figure 10) including average (ave) and standard deviation (SD; $\pm 1\sigma$) data for like regions.

Region	О	Na	Al	P	K	Fe	Sr	Cs	Ce	Nd
reg-1	63.5	1.3	9.2	15.0	4.4	4.8	1.0	0.3	0.3	0.2
reg-2	63.7	1.3	9.0	15.0	4.5	4.7	1.1	0.4	0.2	0.2
reg-3	63.6	1.2	9.1	15.2	4.4	4.7	1.0	0.4	0.2	0.1
reg-4	63.1	1.3	9.2	15.3	4.4	4.9	1.0	0.3	0.4	0.2
reg-5	63.6	1.2	9.1	15.2	4.3	4.7	1.0	0.3	0.3	0.2
ave	63.5	1.3	9.1	15.2	4.4	4.8	1.0	0.3	0.3	0.2
SD	0.2	0.0	0.1	0.1	0.1	0.1	0.0	0.1	0.1	0.0



Figure 11. SEM micrograph with EDS spot analysis regions for G3 at the top of the sample near the phase-separated region (low magnification) with the data presented in Table 8.

Table 8. Summary of EDS spot analysis results (atomic%) from the top (high magnification) region of G3 (see Figure 11).

Region	О	Na	Al	P	K	Fe	Sr	Cs	Ce	Nd
reg-1	63.7	0.3	13.5	14.8	1.6	4.7	1.1	0.1	0.2	0.2
reg-2	63.9	0.4	12.5	14.6	1.6	5.3	1.2	0.1	0.2	0.2
reg-3	63.9	0.3	12.2	14.3	1.8	5.6	1.4	0.1	0.2	0.2
reg-4	65.1	0.0	4.8	13.1	8.1	7.5	0.0	0.5	0.5	0.3
reg-5	63.4	1.2	10.4	14.1	4.6	4.5	1.0	0.4	0.2	0.2
reg-6	63.3	1.2	10.1	14.6	4.5	4.5	1.1	0.3	0.3	0.2

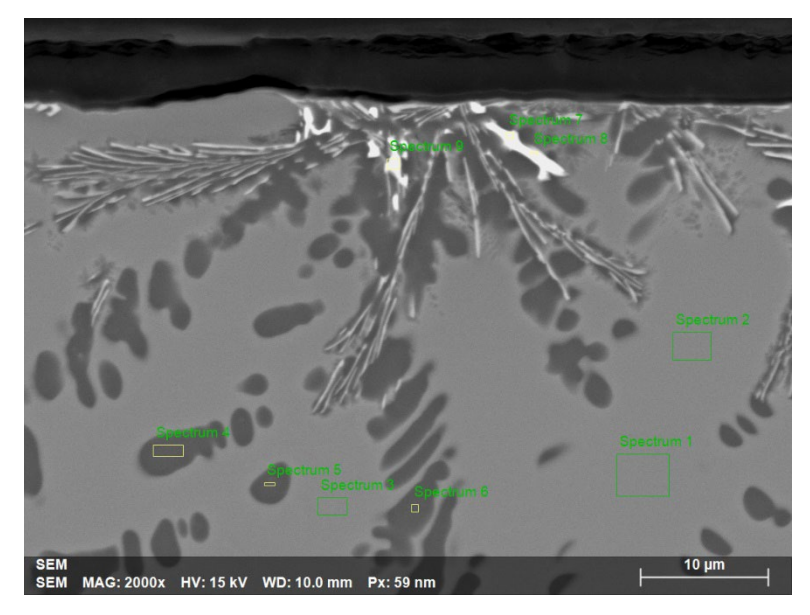


Figure 12. SEM micrograph with EDS spot analysis regions for G3 at the top of the sample near the phase-separated region (high magnification), including some dendritic crystal growth, with data included in Table 9.

Table 9. Summary of EDS spot analysis results (atomic%) from G3 (see Figure 12) with separate datasets for the matrix phase (light gray – regions 1-3), dark gray phase (regions 4-6), and the bright phase at the top (regions 7-9) including average (ave) and standard deviations (SD; $\pm 1\sigma$) for the like regions.

Desc.	Region	0	Na	Al	P	K	Fe	Sr	Cs	Ce	Nd
gray phase	reg-1	65.3	1.6	7.4	14.3	4.9	4.8	1.0	0.4	0.2	0.2
	reg-2	66.4	1.7	6.4	14.0	4.7	4.9	1.0	0.4	0.2	0.2
ht g ix p	reg-3	65.1	1.6	7.3	14.3	4.9	5.0	1.0	0.4	0.2	0.2
Light gray matrix phas	ave	65.6	1.6	7.0	14.2	4.9	4.9	1.0	0.4	0.2	0.2
n	SD	0.7	0.1	0.5	0.2	0.1	0.1	0.0	0.0	0.0	0.0
	reg-4	65.6	0.1	15.6	15.8	0.5	1.0	1.0	0.1	0.1	0.1
ray	reg-5	65.2	0.2	15.4	16.1	0.7	1.0	1.2	0.1	0.1	0.1
Dark gray phase	reg-6	65.7	0.2	14.6	15.2	1.2	1.6	1.1	0.1	0.1	0.1
Da _l	ave	65.5	0.2	15.2	15.7	0.8	1.2	1.1	0.1	0.1	0.1
	SD	0.3	0.0	0.6	0.4	0.3	0.3	0.1	0.0	0.0	0.0
Bright phase	reg-7	66.1	0.5	6.1	15.4	0.9	1.0	1.6	0.2	4.7	3.4
	reg-8	67.3	0.0	1.6	13.8	2.2	1.7	0.0	0.4	7.6	5.3
	reg-9	69.5	0.0	4.6	12.5	2.2	6.7	0.0	0.3	2.7	1.5
	ave	67.6	0.2	4.1	13.9	1.8	3.1	0.6	0.3	5.0	3.4
Щ	SD	1.7	0.3	2.3	1.4	0.7	3.1	0.9	0.1	2.5	1.9

Additionally, XRD data for the bulk G3 sample is provided in Figure 13 where no crystalline diffraction peaks were observed. It is clear that crystalline material is likely present in some of these pieces, but likely these concentrations are below the instrument detection limit.

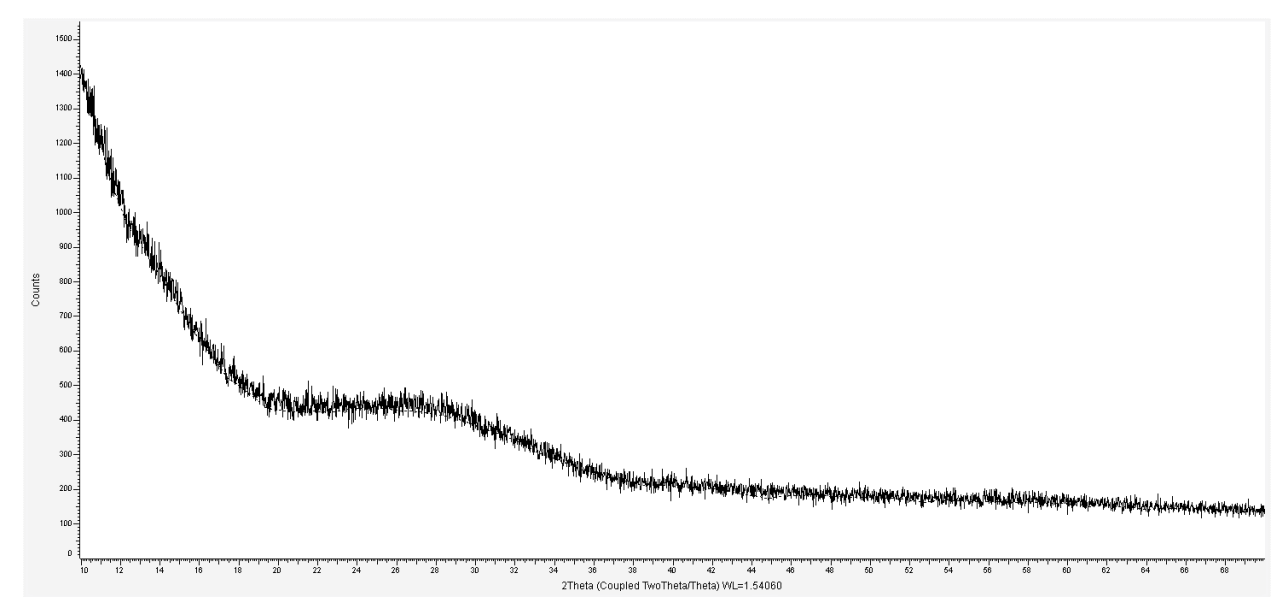


Figure 13. XRD data for the quenched G3 sample after vitrification. While monazite-type crystals were observed during SEM-EDS analysis, these are below detection limits of the XRD instrument.

4.3 Results for Sample G5

The SEM-EDS data for Sample-G5 are provided in Figure 14, Figure 15, Figure 16 as well as Table 10. The matrix of G5 was homogeneous with phase separation observed at the top of the quenched material. The higher magnification $(2k\times)$ SEM micrograph provided in Figure 14c shows three distinct phases based on visual appearance. At a high-level, EDS spot analysis of the homogeneous matrix phase and the phase-separated region did not show statistically different compositions (see Figure 16 and Table 10). The dark phase seen in Figure 14c and Figure 15 appeared higher in Al_2O_3 concentration than the bulk phase based on the EDS dot map (see Figure 15) and XRD analysis in Figure 17 showed the presence of AlPO₄, so it is presumed that this dark phase is AlPO₄.

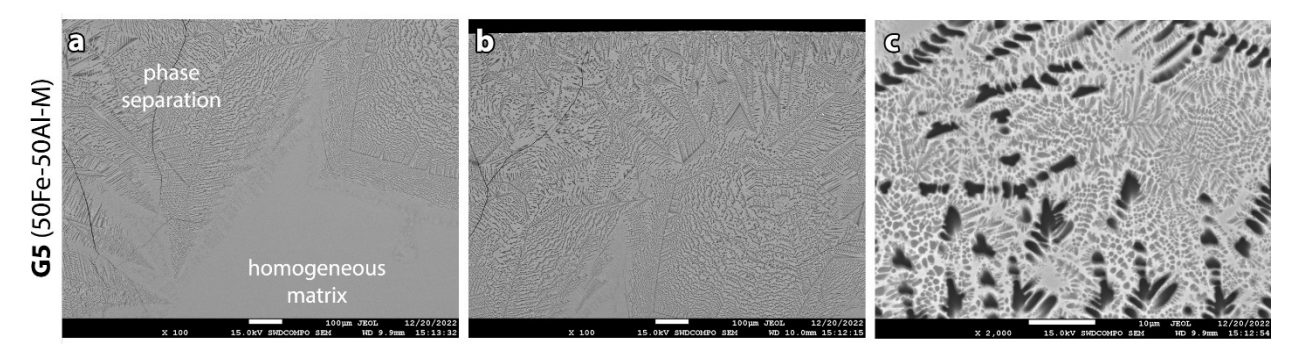


Figure 14. SEM micrographs for G5 at (a) 100× (middle), (b) 100× (top), and (c) 2000× (top) magnifications.

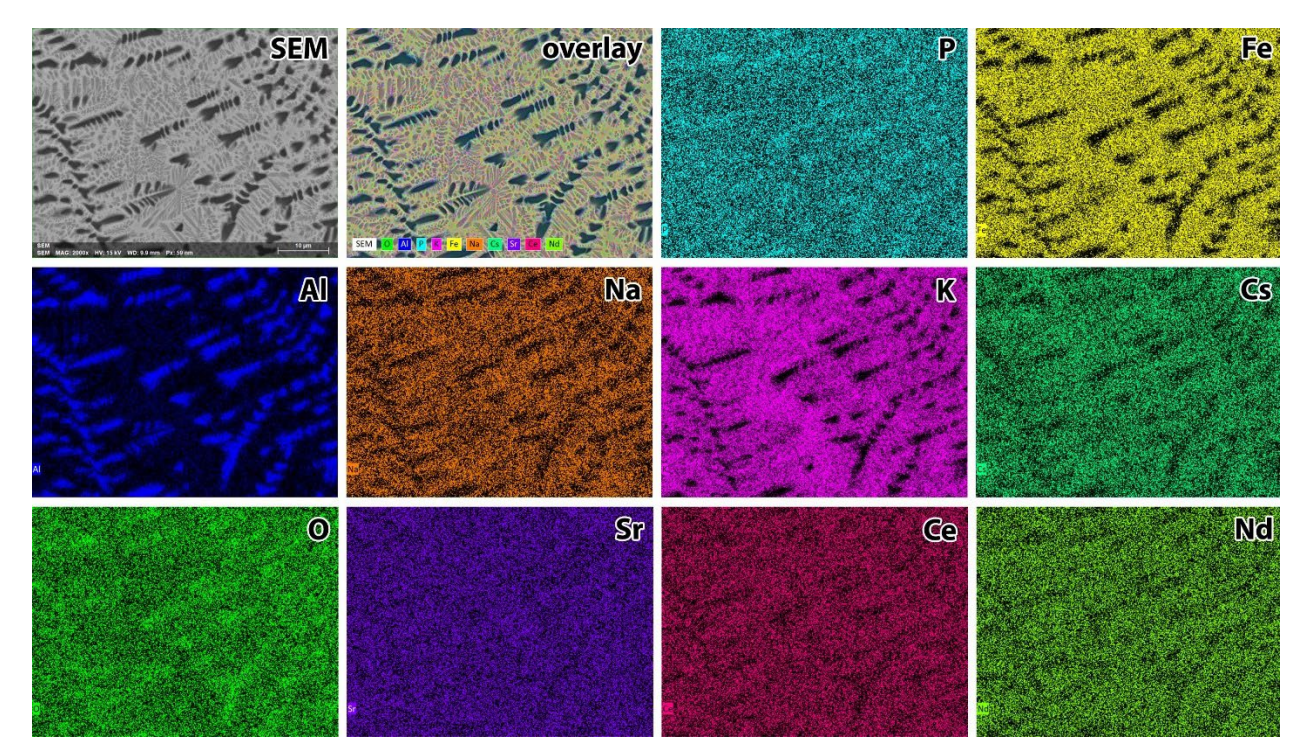


Figure 15. SEM-EDS dot map for G5 including the SEM micrograph, EDS overlay, and the elemental maps for P, Fe, Al, Na, K, Cs, O, Sr, Ce, and Nd.

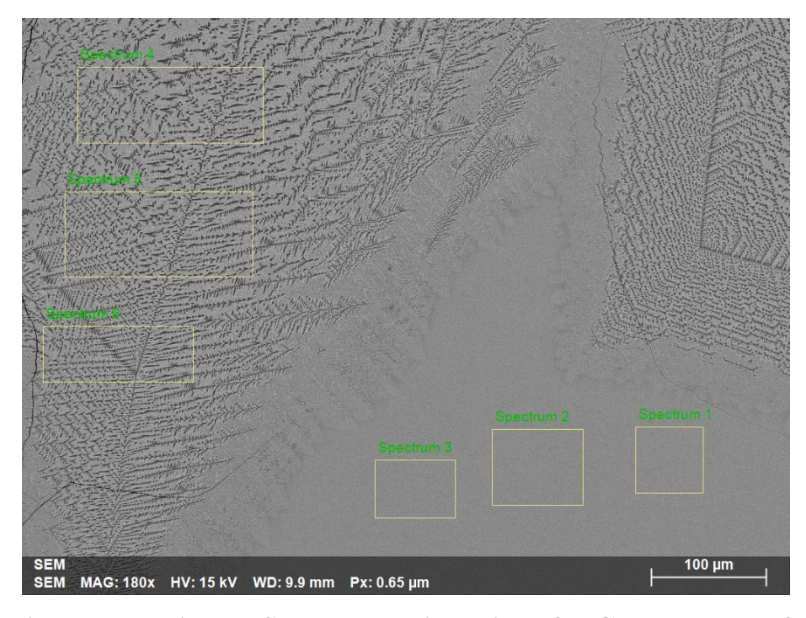


Figure 16. SEM micrograph with EDS spot analysis regions for G5 at the top of the sample where the phase separation meets the bulk matrix phase with data presented in Table 10.

Table 10. Summary of EDS spot analysis results (atomic%) from G5 (see Figure 16) including the homogeneous matrix phase (regions 1-3) and the heterogeneous and phase-separated region (regions 4-6) including average (ave) and standard deviation (SD; $\pm 1\sigma$) data for like regions.

Desc.	Region	0	Na	Al	P	K	Fe	Sr	Cs	Ce	Nd
Homogeneous matrix phase	reg-1	63.1	1.4	7.1	16.3	4.8	5.3	1.1	0.2	0.4	0.2
	reg-2	63.2	1.5	7.2	16.2	4.6	5.4	1.1	0.2	0.4	0.2
oger ix p	reg-3	63.8	1.3	7.1	15.9	4.7	5.3	1.0	0.4	0.2	0.2
ome	ave	63.4	1.4	7.2	16.1	4.7	5.3	1.1	0.3	0.3	0.2
Ш 1	SD	0.4	0.1	0.0	0.2	0.1	0.0	0.0	0.1	0.1	0.0
eq	reg-4	63.4	1.3	7.4	16.0	4.7	5.2	1.1	0.3	0.4	0.2
arat n	reg-5	63.3	1.3	7.6	16.1	4.6	5.2	1.1	0.2	0.4	0.2
Phase-separated region	reg-6	63.3	1.2	7.4	16.0	4.8	5.4	1.0	0.3	0.3	0.2
	ave	63.3	1.3	7.5	16.1	4.7	5.3	1.1	0.3	0.4	0.2
	SD	0.1	0.1	0.1	0.0	0.1	0.1	0.0	0.0	0.0	0.0

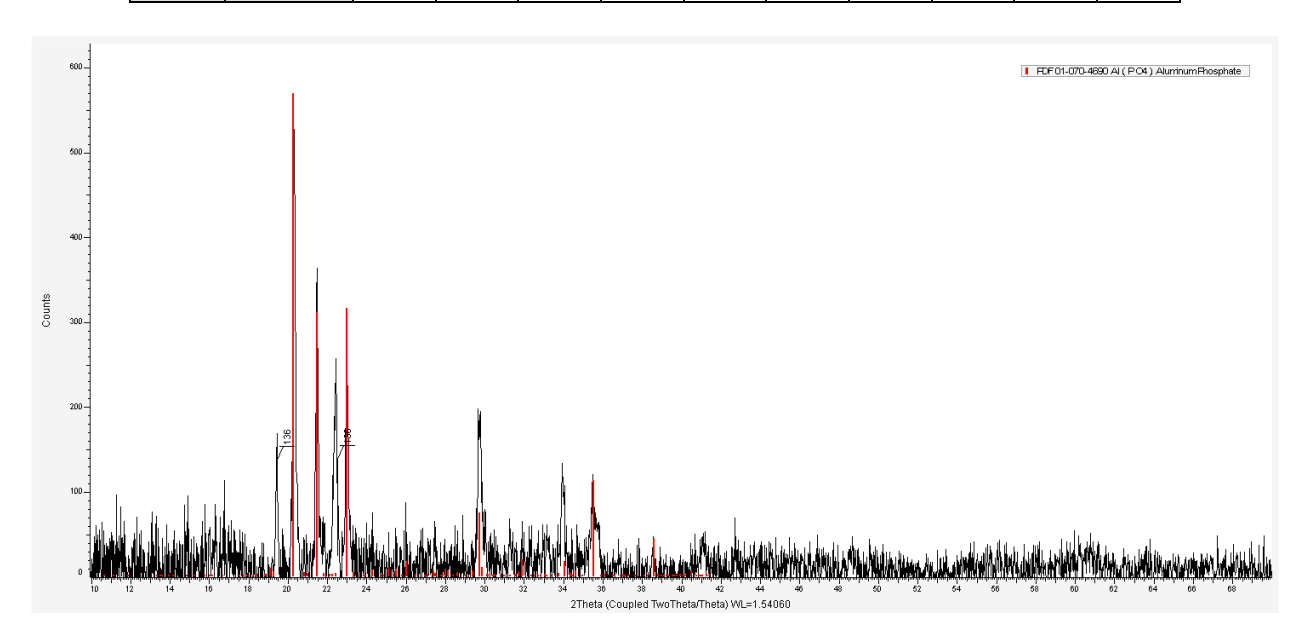


Figure 17. XRD data for the quenched G5 sample after vitrification (peaks at 19.5° 2θ, 22.5° 2θ, and 34° 2θ remain unidentified).

4.4 Results for Sample G6

The SEM-EDS data for Sample-G6 are provided in Figure 18, Figure 19, and Figure 20 as well as Table 11 and show a two-phase material with a homogeneous matrix phase and what appear to be pockets of AlPO₄ based on the EDS data (Table 11) and the XRD data provided in Figure 21. These AlPO₄ patches appear fractured, and this is likely due to a mismatch in the thermal expansion coefficients of these phases where the cracking occurred during the quenching process.

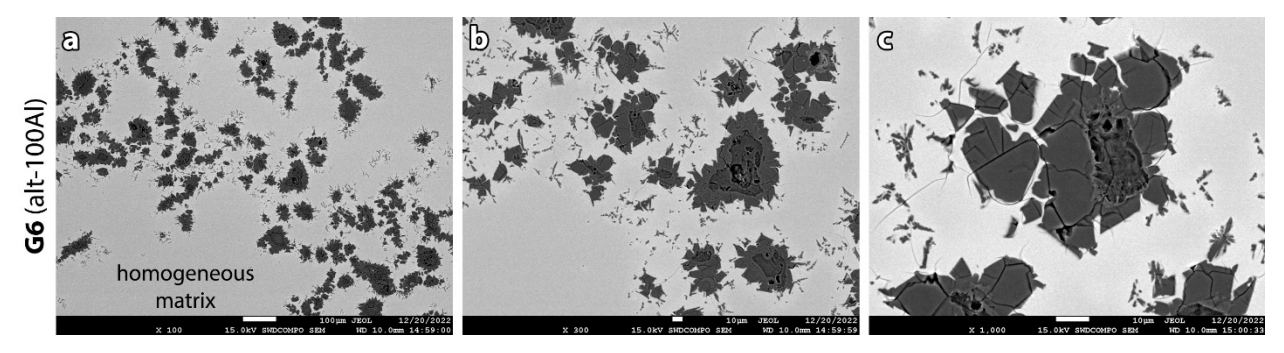


Figure 18. SEM micrographs for G6 at (a) 100×, (b) 300×, and (c) 1000× magnifications.

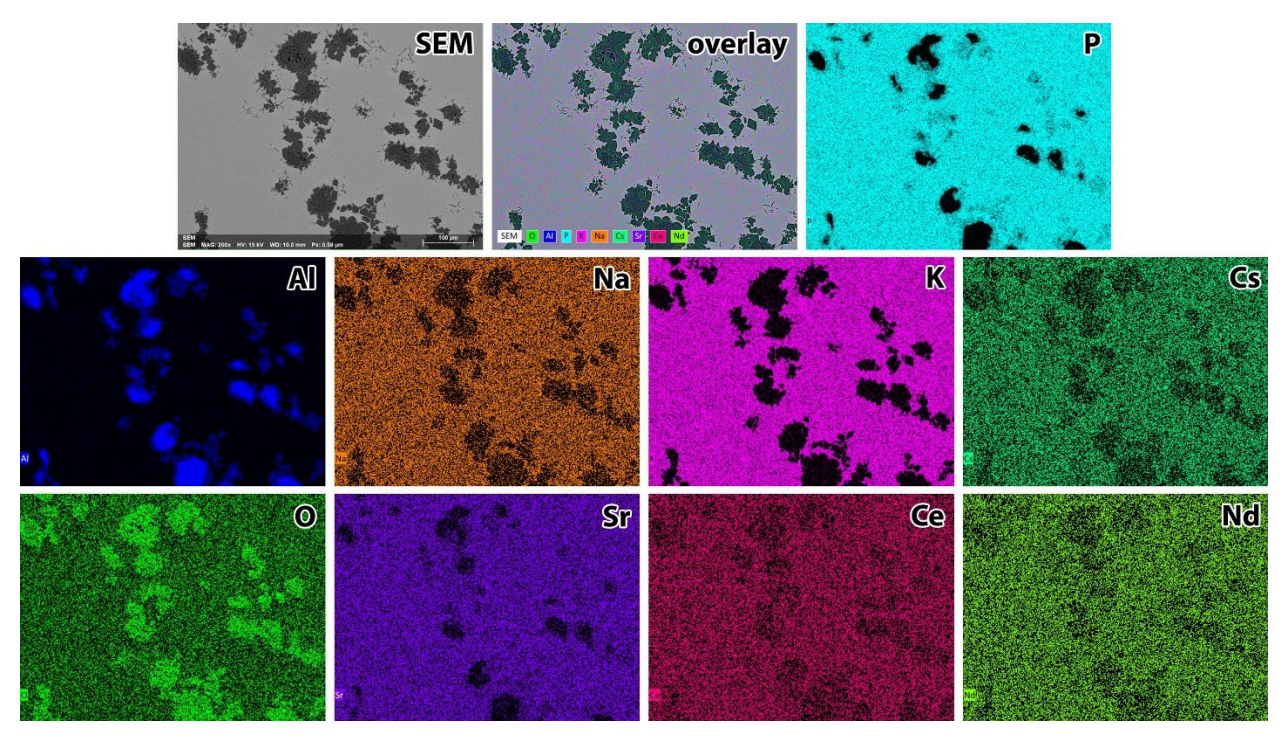


Figure 19. SEM-EDS dot map for G6 including the SEM micrograph, EDS overlay, and the elemental maps for P, Fe, Al, Na, K, Cs, O, Sr, Ce, and Nd.

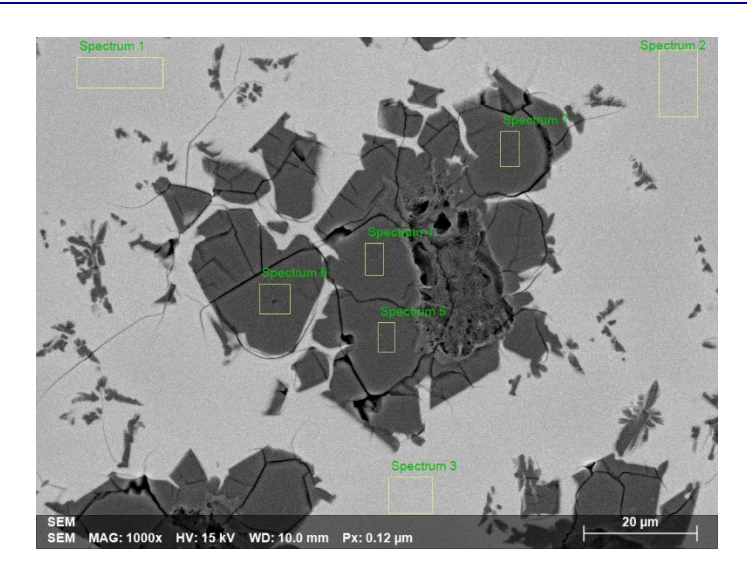


Figure 20. SEM micrograph with EDS spot analysis regions for G6 in the middle of the sample where the light matrix phase is distinctly different from the dark (AlPO₄) inclusion phases – EDS data is presented in Table 11.

Table 11. Summary of spot EDS data (atomic%) for G6 with regions called out in Figure 20 including average (ave) and standard deviation (SD; $\pm 1\sigma$) data for like regions.

Reg#	О	Na	Al	P	K	Sr	Cs	Ce	Nd
1	68.6	0.0	2.3	19.1	8.4	0.2	0.4	0.7	0.4
2	66.5	1.2	6.2	20.0	4.1	1.3	0.3	0.2	0.2
3	66.2	1.5	5.0	20.7	4.5	1.3	0.2	0.3	0.2
ave	67.1	0.9	4.5	19.9	5.7	0.9	0.3	0.4	0.3
SD	1.3	0.8	2.0	0.8	2.4	0.7	0.1	0.2	0.1
4	65.4	0.0	17.8	15.6	0.0	0.9	0.1	0.1	0.1
5	65.3	0.1	17.9	15.6	0.1	0.9	0.0	0.0	0.1
6	65.4	0.1	17.7	15.3	0.0	1.0	0.3	0.1	0.2
7	65.8	0.0	17.5	15.3	0.1	0.9	0.1	0.1	0.1
ave	65.5	0.0	17.7	15.4	0.1	0.9	0.1	0.1	0.1
SD	0.2	0.0	0.1	0.2	0.0	0.0	0.1	0.0	0.0

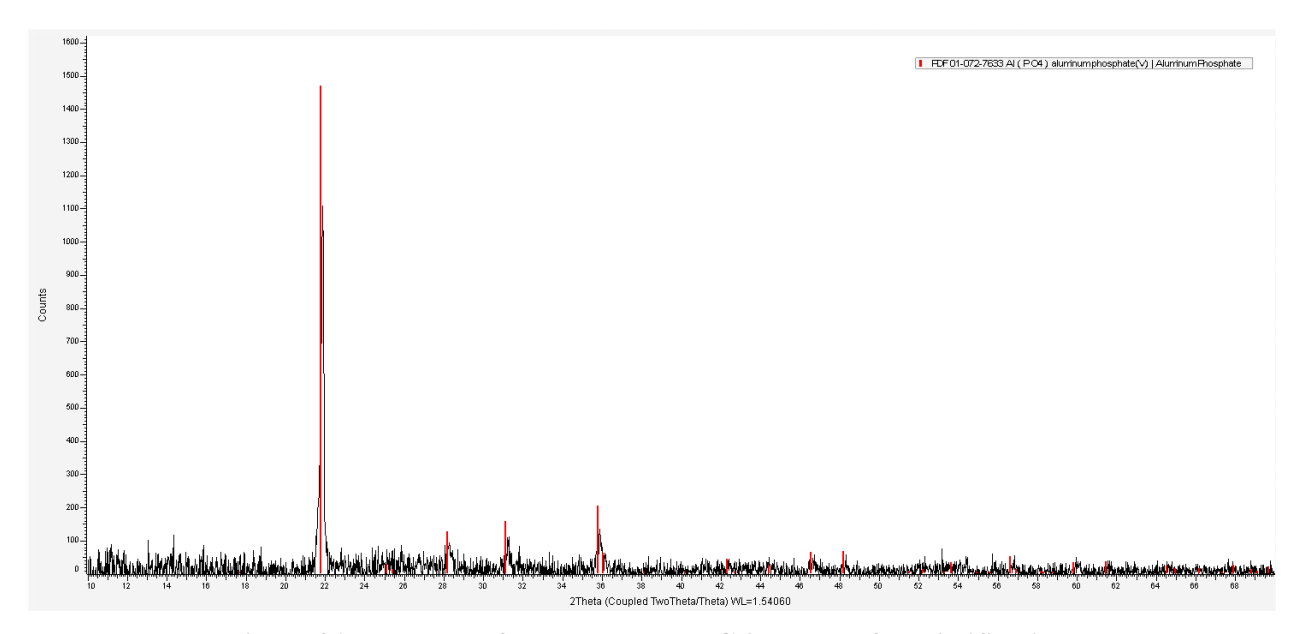


Figure 21. XRD data for the quenched G6 sample after vitrification.

An additional picture of G6 is provided in Figure 22 that shows the true color of this material on a white background, which is a light blueish purple. This color is not apparent with the black background shown in Figure 3.



Figure 22. Picture of G6 on white background so the blueish-purple color is easier to observe.

5.0 Summary and Conclusions

The goal of this work was to evaluate higher-Al₂O₃ phosphate glasses for comparison with the Fe₂O₃-phosphate formulations from our previous work with ERV2 and ERV3b salt simulants because many literature studies suggest that the addition of Al₂O₃ to phosphate melts improves glass properties including chemical durability. In this study, we reviewed the available literature on this topic to establish a foundation of knowledge for the formulation portion to follow. Through the literature survey, several iron aluminophosphate studies were found and were used as a starting point for the experimental work.

While several studies have been performed on the iron phosphate reference waste form composition (called DPF5-336) being established under the Material Recovery and Waste Form Development Campaign under this work, it has been made under many different conditions including at different batch sizes, with different salt compositions, at different melting temperatures, and using different processing approaches (i.e., starting from salt, starting from oxides/carbonates of the salt cations, using different dechlorination apparatuses). Thus, the DPF5-336 was made in the current study starting from oxides and carbonates of the salt cations. This approach of using oxides and carbonates of the salt cations was used for all glasses in the current study because of the limited availability of the ERV3b salt simulant. In this study, four glasses were produced that included one Al₂O₃-free glass (G1, the DPF5-336 reference glass), two iron aluminophosphate (Al₂O₃/Fe₂O₃-containing) glasses (i.e., G3 and G5), and an aluminophosphate (Fe₂O₃-free) glass (G6).

All four samples were characterized with optical photographs as well as SEM-EDS and XRD analyses. Each sample had some type of phase separation and/or crystallization based on appearances (optically or with the SEM) or on the diffraction data alone. Samples G1, G3, G5, and G6 had phases of Li₃Fe₂(PO₄)₃ (likely), monazite (below XRD detection limits), AlPO₄, and AlPO₄, respectively.

These samples were shipped to Argonne National Laboratory for chemical durability testing using the ASTM C1308 testing procedure. Once these tests are conducted, a phase-II approach could be used to further pursue aluminophosphate compositions within this compositional space.

6.0 Acknowledgements

The authors acknowledge support on this work from John Vienna, Xiaonan Lu, and Charmayne Lonergan (PNNL), William Ebert and Sarah Stariha (ANL), Steve Frank, Steve Herrmann, Ken Marsden, Morgan Kropp, and Kevin Tolman (INL), Professor Krista Carlson (University of Nevada Reno), Professor Michael Simpson (University of Utah), Professor Richard Brow (Missouri University of Science and Technology), CW Kim (MoSci Corporation), and Ming Tang (Clemson University). Authors also acknowledge support on the DOE-NE Material Recovery and Waste Form Campaign from Ken Marsden (INL), Kimberly Gray (DOE-NE), James Willit (DOE-NE), and Stephen Kung (DOE-NE). The university collaborations were performed through the Nuclear Energy University Partnership (NEUP) Program under DOE-NE.

7.0 References

Bateman KJ, CJ Knight, CW Solbrig. 2007. *Current Status of Ceramic Waste Form Development*. INL/INT-06-11736, Rev. 1, Idaho National Laboratory, Idaho Falls, Idaho.

Brow RK. 1993. "Nature of alumina in phosphate glass: I, properties of sodium aluminophosphate glass." *Journal of the American Ceramic Society* **76**(4):913-918.

Chenu S, U Werner-Zwanziger, C Calahoo, JW Zwanziger. 2012. "Structure and properties of NaPO₃-ZnO-Nb₂O₅-Al₂O₃ glasses." *Journal of Non-Crystalline Solids* **358**(15):1795-1805.

Donald IW, BL Metcalfe, SK Fong, LA Gerrard. 2006. "The influence of Fe₂O₃ and B₂O₃ additions on the thermal properties, crystallization kinetics and durability of a sodium aluminum phosphate glass." *Journal of Non-Crystalline Solids* **352**(28-29):2993-3001.

Ebert WL. 2005. Testing to Evaluate the Suitability of Waste Forms Developed for Electrometallurgically-Treated Spend Sodium-Bonded Nuclear Fuel for Disposal in the Yucca Mountain Repository. ANL-05/43, Argonne National Laboratory-East, Argonne, Illinois.

Ebert WL. 2022. Conceptual Iron Phosphate Waste Form Degradation Model. ANL/CFCT-22/48. Argonne National Laboratory, Lemont, Illinois.

Ebert WL, BJ Riley, SM Frank. 2017. *Test Plan for Salt Treatment and Waste Form Development*. NTRD-MRWFD-2017-000191, Argonne National Laboratory, Lemont, Illinois.

Ebert WL, JA Fortner. 2019a. Analysis of Iron Phosphate Glasses for Dehalogenated Salt Waste. ANL/CFCT-19/5, Argonne National Laboratory, Lemont, Illinois.

Ebert WL, JA Fortner. 2019b. Corrosion Tests with Developmental Iron Phosphate Glass Waste Forms. ANL/CFCT-19/7, Argonne National Laboratory, Lemont, Illinois.

El Damrawi G, AK Hassan, A Shahboub. 2020. "Chemical durability and structure of Al₂O₃-Ag₂O-P₂O₅ glasses." *Applied Physics A* **126**(4):1-7.

El Hadrami A, H Aouad, M Mesnaoui, A Maazaz, J-J Videau. 2002. "Storage of toxic heavy metals in phosphate glasses: physical and water durability properties." *Materials Letters* **57**(4):894-898.

El Hadrami A, M Mesnaoui, M Maazaz, J-J Videau. 2003. "Kinetic dissolution of phosphate glasses containing toxic heavy metals." *Journal of Non-Crystalline Solids* **331**(1-3):228-239.

Frank SM, BJ Riley, W Ebert, JA Peterson. 2017. *Literature Review of Dehalogenation Processes for Salt Wastes and Suitable Waste Forms*. NTRD-MRWFD-2017-000193, Idaho National Laboratory, Idaho Falls, Idaho.

Glazkova IS, SN Kalmykov, IA Presniakov, AV Sobolev, OI Stefanovsky, SV Stefanovsky, SE Vinokurov, BF Myasoedov. 2017. "Iron oxidation state and coordination, and hydrolytic durability of sodium-aluminum iron phosphate glasses." *Progress in Nuclear Energy* **94**:235-239.

Hrma PR. 2010. Retention of Halogens in Waste Glass. PNNL-19361, Pacific Northwest National Laboratory, Richland, Washington.

Kapoor S, RE Youngman, L Ma, N Lönnroth, SJ Rzoska, M Bockowski, LR Jensen, M Bauchy, MM Smedskjaer. 2019. "Permanent densification of calcium aluminophosphate glasses." *Frontiers in Materials* **6**:63.

Karabulut M, E Melnik, R Stefan, GK Marasinghe, CS Ray, CR Kurkjian, DE Day. 2001a. "Mechanical and structural properties of phosphate glasses." *Journal of Non-Crystalline Solids* **288**(1-3):8-17.

Karabulut M, E Metwalli, RK Brow. 2001b. "Structure and properties of lanthanum-aluminum-phosphate glasses." *Journal of Non-Crystalline Solids* **283**(1-3):211-219.

Li S, S Huang, F Wu, Y Yue. 2015. "Structure and properties of zinc aluminophosphate glasses and those doped with zirconium dioxide." *Journal of Non-Crystalline Solids* **419**:45-50.

Liu H, Y Lu, Y Qu, H Lu, Y Yue. 2016. "Effect of the content of Al₂O₃ on structure and properties of calcium-phosphate glasses: two experimental case studies." *Journal of Non-Crystalline Solids* **450**:95-102.

Marino AE, SR Arrasmith, LL Gregg, SD Jacobs, G Chen, Y Duc. 2001. "Durable phosphate glasses with lower transition temperatures." *Journal of Non-Crystalline Solids* **289**(1-3):37-41.

Metwalli E, RK Brow. 2001. "Modifier effects on the properties and structures of aluminophosphate glasses." *Journal of Non-Crystalline Solids* **289**(1-3):113-122.

Moreau F, A Durán, and F Muñoz. 2009. "Structure and properties of high Li₂O-containing aluminophosphate glasses." *Journal of the European Ceramic Society* **29**(10):1895-1902.

Riley BJ, BT Rieck, JS McCloy, JV Crum, SK Sundaram, JD Vienna. 2012. "Tellurite glasses as a waste form for mixed alkali chloride waste streams: Candidate materials selection and initial testing." *Journal of Nuclear Materials* **424**:29-37.

Riley BJ, JA Peterson, JD Vienna, WL Ebert, SM Frank. 2020. "Dehalogenation of electrochemical processing salt simulants with ammonium phosphates and immobilization of salt cations in an iron phosphate glass waste form," *Journal of Nuclear Materials* **529**:151949.

Riley BJ, JD Vienna, SM Frank, JO Kroll, JA Peterson, NL Canfield, Z Zhu, J Zhang, K Kruska, DK Schreiber. 2017. "Glass binder development for a glass-bonded sodalite ceramic waste form." *Journal of Nuclear Materials* **489**:42-63.

Riley BJ, MJ Schweiger, D-S Kim, WW Lukens, BD Williams, C Iovin, CP Rodriguez, NR Overman, ME Bowden, DR Dixon, JV Crum, JS McCloy, AA Kruger. 2014. "Iodine solubility in low-activity waste borosilicate glass at 1000°C." *Journal of Nuclear Materials* **452**(1-3):178-188.

Riley BJ, S Chong. 2020. Completion of Milestone M4FT-20PN030105031: Evaluate physical properties of CCC-cooled phosphate glass waste forms. PNNL-SA-155636, Pacific Northwest National Laboratory, Richland, Washington.

Riley BJ, S Chong, C Lonergan, C Skidmore. Personal communication. 2019. *Completion of Milestone M4FT-19PN030105073 - Send glasses to ANL for durability testing (PNNL-ANL)*. Pacific Northwest National Laboratory, Richland, Washington.

Riley BJ, S Chong. 2022a. Completion of Milestone M3FT-22PN030104041: Ship iron phosphate glass to ANL for chemical durability testing." PNNL-SA-173625, Pacific Northwest National Laboratory, Richland, Washington.

Riley BJ, S Chong. 2022b. "Effects of composition and canister centerline cooling on microstructure, phase distribution, and chemical durability of dehalogenated iron phosphate waste forms," *Journal of Non-Crystalline Solids* **579**:121319.

Riley BJ, S Chong, CE Lonergan. 2021. "Dechlorination apparatus for treating chloride salt wastes: System evaluation and scale-up," *ACS Omega* **6**(47):32239-32252.

Riley BJ, S Chong, ET Nienhuis. 2023. *Canister Centerline Cooling Experiments for DPF5-336 Reference Material Made with ERV3b Salt Simulant*. PNNL-33802, Pacific Northwest National Laboratory, Richland, Washington.

Siemer DD. 2012. "Improving the integral fast reactor's proposed salt waste management system." *Nuclear Technology* **178**(3):341-352.

Stariha S, WL Ebert. 2020. Corrosion Behavior of Developmental Iron Phosphate Waste Forms: FY20 Status Report. ANL/CFCT-20/34, Argonne National Laboratory, Lemont, Illinois.

Stariha S, WL Ebert. 2021. Corrosion Behavior of Developmental Iron Phosphate Waste Forms: FY21 Status Report. ANL/CFCT-21/14, Argonne National Laboratory, Lemont, Illinois.

Stariha S, WL Ebert. 2022. Corrosion Behavior of Fast-Cooled Iron Phosphate Reference Material. ANL/CFCT-22/49, Argonne National Laboratory, Lemont, Illinois.

Teixeira Z, OL Alves, and IO Mazali. 2007. "Structure, thermal behavior, chemical durability, and optical properties of the Na₂O-Al₂O₃-TiO₂-Nb₂O₅-P₂O₅ glass system." *Journal of the American Ceramic Society* **90**(1):256-263.

Vienna JD, ED Collins, JV Crum, WL Ebert, SM Frank, TG Garn, D Gombert, R Jones, RT Jubin, VC Maio, JC Marra, J Matyas, TM Nenoff, BJ Riley, GJ Sevigny, NR Soelberg, DM Strachan, PK Thallapally, JH Westsik. 2015. *Closed Fuel Cycle Waste Treatment Strategy*. FCRD-MRWFD-2015-000674, PNNL-24114, Pacific Northwest National Laboratory, Richland, Washington.

Appendix A:

XRD Information

Table A1. Summary of phases identified during XRD analysis including the powder diffraction file (PDF) numbers from the ICDD database, the space group (SG; and SG number), and the unit cell parameters in Angstroms (Å).

Commla	Dhaga	PDF#	SC (#)	Unit cell parameters (Å)				
Sample	Phase	PDr#	SG (#)	а	b	С		
G1	$Li_3Fe_2(PO_4)_3$	00-053-1027	R-3 (148)	8.30900	8.30900	22.46200		
G5	AlPO ₄	01-070-4690	<i>Pc</i> (7)	37.3863	5.0455	26.2217		
G6	AlPO ₄	01-072-7633	C2221 (20)	7.08430	7.08230	6.99890		

Appendix B:

Milestone Details

The details of this milestone are the following:

- Milestone Number: M4FT-23PN030104041.
- Title: Make aluminophosphate waste form(s) and send to ANL for future testing
- **Description**: This work will be initiated by a literature review assessing the state of aluminophosphate research. Based on this review, at least one composition (containing Al-P-O) will be produced and characterized. The product(s) will be characterized and sent to ANL for future testing.
- **Due Date**: 03/31/2023
- **Criteria for Completion**: A memorandum will be sent to the FM, NTD, and CAM summarizing this work. (*Note that a technical report also meets the qualifications of criteria for completion*.)
- Work Package: FT-23PN03010404
- Work Package Title: Off-Gas & Waste Forms PNNL
- Work Breakdown Structure: 1.02.03.01.04